ACS APPLIED MATERIALS & INTERFACES

Functional Nanostructured Materials (including low-D carbon)

Strontium doped bioactive glass nanoparticles in osteogenic commitment

Alvaro J. Leite, Ana I. Gonçalves, Marcia T Rodrigues, Manuela E. Gomes, and João F. Mano

ACS Appl. Mater. Interfaces, **Just Accepted Manuscript** • DOI: 10.1021/acsami.8b06154 • Publication Date (Web): 15 Jun 2018

ACS Publications

is published by the American Chemical Society. 1155 Sixteenth Street N.W., Washington, DC 20036

Strontium doped bioactive glass nanoparticles in osteogenic commitment

Álvaro J. Leite[1,2], Ana I. Gonçalves[1,2], Márcia T. Rodrigues[1,2], Manuela E. Gomes[1,2,3], João F. Mano[1,2,4,]*

1 - 3B's Research Group - Biomaterials, Biodegradables and Biomimetics, University of Minho, Headquarters of the European Institute of Excellence on Tissue Engineering and Regenerative Medicine, Avepark- Parque de Ciência e Tecnologia, 4805-017- Barco, Guimarães, Portugal

2 - ICVS/3B's - PT Government Associate Laboratory, Braga/Guimarães, Portugal

3 - The Discoveries Centre for Regenerative and Precision Medicine, Headquarters at University of Minho, Avepark, 4805-017 Barco, Guimarães, Portugal

4 - Present address: Department of Chemistry, CICECO – Aveiro Institute of Materials, University of Aveiro, 3810-193 Aveiro, Portugal. E-mail: jmano@ua.pt

* - Corresponding Author

KEYWORDS

Nanoparticles, Bioactivity, Osteogenic Commitment, Strontium, Sol-Gel

ABSTRACT

The present work explores bioactive glass nanoparticles (BGNPs) and developed strontium−doped nanoparticles (BGNPsSr), envisioning orthopedic strategies compatible with vascularization. The nanoparticles were synthesized by sol−gel, achieving a diameter of 55 nm for BGNPs and of 75 nm for BGNPsSr, and the inclusion of strontium caused none structural alteration. The nanoparticles exhibited high cytocompatibility for HUVECs and SaOS−2. Additionally, the incorporation of strontium emphasized the tubule networking behavior of HUVECs. Our results demonstrate that the nanoparticles dissolution products encouraged the osteogenic differentiation of hASCs as it favored the expression of key genes and proteins associated with the osteogenic lineage. This effect was markedly enhanced for BGNPsSr, that could prompt stem cell osteogenic differentiation without the typical osteogenic inducers. This study not only supports the hypothesis that bioactive glass nanoparticles might play a significant role in osteogenic commitment but also highlights that the designed BGNPsSr is a valuable tool for stem cell “tune-up” in bone tissue engineering applications.

INTRODUCTION

Traumatic injuries, infections or tumor resections can originate critical-sized bone defects that cannot regenerate *per se*. The current treatments using autografts or allografts are limited due to recurrent second site surgery, donor site morbidity, limited availability, immunological rejection, disease transmission, high costs, and limited integration with natural bone. In this regard, bioactive glasses find use as a standard alternative for allografts in orthopedic treatments due to their excellent tissue integration.[1-2] Upon implantation into bone defects, they can induce a bone-like apatite layer on their surface, stimulate osteogenesis, angiogenesis, and promote high osteoinduction rates.[3-4] These features are crucial for an interfacial bonding between the bone and the implant, leading to osteointegration.[5] However, their outcome is unsatisfactory compared to biological grafts, and bone tissue regeneration requires materials that mimic the natural bone nanostructured niche.[6]

It was also found that the communications between cells and biomaterials occur on the nanoscale.[7] At this level, several interrelated properties regulate the cell-biomaterial interactions such as nanotopography, surface area, energy, hydrophilicity, or chemical composition.[8-9] These features govern the contacts with proteins, modulate cell adhesion, spreading, proliferation and, at last, they affect the long-term functionality of implants.[10-11] Thus, in recent years, nanotechnology tools have been explored to develop bioactive glass nanoparticles (BGNPs).[12] Indeed, the use of nano-sized bioactive glass offers advantages over bulk bioactive glasses once they maximize the surface area, enhance the dissolution of the ions, amplify *in vitro* bioactivity, and improve mechanical properties of nanocomposites when used as filler material.[13-14] Composites based on polymers and BGNPs could mimic the natural bone structure, as organic

and inorganic phases compose the extracellular matrices of hard tissues, showing potential for bone tissue engineering and periodontal regeneration.[15] Thus, the nanoparticulate form of bioactive glasses could be an ideal bioactive 'nanocomponent' for bone scaffolds.[16-17]

The ionic constituents of the glass network could enhance the therapeutic performance of bioactive glasses.[18] Therefore, there is a high demand to develop new BGNPs with a tailored chemical composition for broader applications. In this regard, strontium (Sr) has attracted attention due to its therapeutic effects on orthopedics.[19] Physiologically, Sr is a trace element in human hard tissues that can accumulate in the bone and displace calcium in the apatite phase of bone mineral.[20] Moreover, Sr was correlated with an increase of bone compressive strength and, its deficiency has shown detrimental effects in hard tissues.[21] Sr ions could stimulate bone formation and decrease bone resorption both *in vitro* and *in vivo* being, therefore, used as a pharmaceutical agent for treatment of osteoporosis.[22] Due to its benefits, Sr has been proposed as a therapeutic ion to be incorporated in several bioactive glasses.[18] Also, Sr-containing bioactive glasses stimulated osteogenic differentiation of periodontal ligament cells,[23] mesenchymal stromal cells,[24] and human bone marrow stromal cells.[25] However, typical compositions of bioactive glasses have several components, *e.g.* Na, which is a network modifier that lowers the melting point of the glass.[26] Therefore, when considering BGNPs as a reservoir for the delivery of therapeutic ions, more simple compositions are needed. Minimalistic compositions can be synthesized using the sol-gel process as it enables a control of the reaction kinetics.[27]

Herein, the compositional flexibility of the sol‑gel method was exploited to incorporate strontium (Sr) into ternary based BGNPs in order to improve its biological outcome, without increasing the amount of network modifiers. The developed quaternary strontium doped

bioactive glass nanoparticles (BGNPsSr) have been successfully used in nanocomposite bio-inks in the biofabrication of 3D bioactive structures with proven bioactivity.[28] Consequently, an in-depth knowledge of this nanoparticles became needed. Therefore, this work aimed to study the physicochemical changes of the strontium incorporation, estimate the viability and cellular functionality of relevant cell types, and evaluate the osteogenic potential of the produced nanoparticles unveiling the possible stimulating effects of released Sr ions on stem cells osteogenic differentiation. For this purpose, osteoblast-like cells (SaOS-2) and endothelial-like cells (HUVECs), will be employed for cytocompatibility studies as they are cell types known to be involved in the physiologically bone regeneration process. Hence, human adipose stem cells (hASCs) will be used to mimic the cellular events of the bone formation process, from the stage of osteoprogenitor cell proliferation to the stages of osteogenic maturation. We hypothesized that the BGNPsSr might be effective in the osteogenesis of cells which ultimately contributes to the successful regeneration of bone defects.

RESULTS AND DISCUSSION

PRODUCTION AND CHARACTERIZATION OF THE NANOPARTICLES

By exploiting the flexibility of the sol-gel method, two types of nanoparticles were produced: ternary nanoparticles (BGNPs), and quaternary strontium-doped nanoparticles (BGNPsSr). The conventional sol-gel process (Stöber method) to produce nanoparticles started with the hydrolysis of Si, Ca, P and Sr precursors. Silicon was introduced through the hydrolysis and condensation of TEOS that occurred in an ethanolic medium in the presence of ammonium water. Calcium nitrate and strontium nitrate respectively supplemented calcium and strontium in the formulation. Diammonium hydrogen phosphate was used to add phosphate. Herein, we also used ammonium water to induce precipitation, combining the traditional sol-gel route with co-precipitation methods. **Figure 1A** shows the production steps of the sol-gel method and reveal the characteristic morphology of the produced nanoparticles. Even though the particles appear irregularly shaped, no significant differences in the morphology between the two compositions were found (**Figure S1**). The BGNPs were composed by SiO_2:CaO:P_2O_5 (mol%) = 55:40:5, while the BGNPsSr comprised SiO_2:CaO:P_2O_5:SrO (mol%) = 55:30:5:10 (**Figure 1B, Table S1** and **Figure S2**). The abundance of the identified elements is in agreement with the starting compositions of the sol-gel mixtures used for producing the distinct nanoparticles (**Table S2**). Both nanoparticles presented a heterogeneous size that could vary in the range 40-100 nm for BGNPs and from 30-200 nm for BGNPsSr (**Figure 1C**), denoting that the Sr incorporation slight affects the size of the particles. A possible explanation of the larger particle side could reside in the larger ionic radius of Sr (0.112 nm) compared with Ca (0.099 nm) as replacing calcium with Sr on a molar basis lead to more open silicate networks.[29-31] The nanoparticles composition was

also assessed by FTIR spectroscopy (**Figure 1D**) that showed the bending and stretching vibrations assigned to the silica network existing in bioactive glasses (460 and 810 and 1030 cm^{-1}). The hydro-affinity property of the nanoparticles was investigated by water contact angle and the calculated surface energy (**Figure S3**). Both nanoparticles demonstrated to possess water affinity. This phenomenon could favor the water diffusion and the hydrolytic degradation and the consequent ionic release. Previous studies have reported the water contact angle reduced to 60-65º could favor cell adhesion.[32]

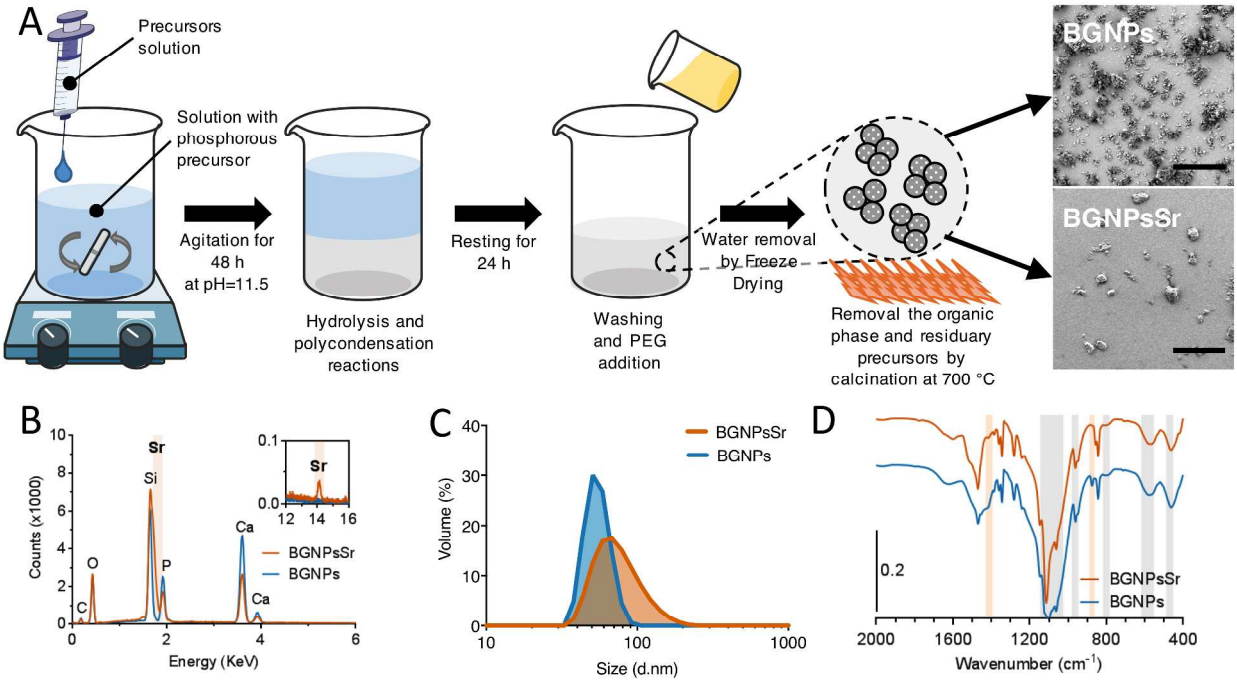

Figure 1. Production scheme and characterization of the developed nanoparticles. **A)** Synthesis of the nanoparticles by sol-gel methodology with SEM micrographs of BGNPs and BGNPsSr. Scale bar = 200 nm. **B)** Identification of chemical elements using EDS. **C)** Evaluation of the size distribution. **D)** FTIR (Fourier-transform infrared) spectra of BGNPs and BGNPsSr.

THE BIOACTIVE BEHAVIOR OF THE NANOPARTICLES

Bearing in mind bone tissue applications, the osteoconductive potential of the nanoparticles was evaluated through biomineralization studies (**Figure 2A**). The formation of a bone-like apatite layer when the material contacts with SBF is an *in vitro* bioactivity indicator of the bioglass tissue interaction in an implant scenario (**Table S3**).[33] One day after immersion in SBF, the samples revealed a rough surface with mineral agglomerates that increased upon 3 days. After 7 days, a dense apatite layer covered the nanoparticles surface showing a typical cauliflower morphology of hydroxyapatite that resulted from the assembling of needle-like crystals (**Figure 2B**). EDS analysis characterized the evolution of the bone-like apatite formation. Herein, the nanoparticles presented a gradual increase in the intensity of both Ca and P peaks accompanied by a steady decrease in the Si and Sr (when applicable) peaks along the 7 days of immersion (**Figure 2C** and **D**). The growth of mineral deposits with increasing incubation time relates to the longer time available for apatite precipitation. Such results indicate the deposition and densification of the apatite layer, agreeing with the SEM images and consistent with previous studies.[34]

Also, the ratio of the Ca and P peaks intensity could indicate the calcification extent (**Figure 2E**). Ca/P ratios were close to the hydroxyapatite stoichiometric theoretical value (1.67) just after 3 days. BGNPsSr exhibits lower peaks of P and Ca than the BGNPs which denote that the Sr doping slightly delays the bioactive behavior of the nanoparticles. However, a faster apatite formation was expected, due to an increased ion dissolution rates potentiated by the expanded network of the Sr-doped BGNPs, that could be the result of the larger atomic size of Sr as compared with Ca.[31] Regarding this opposite effect, it is hypothesized that the ion dissolution

rates are not the leading difference in apatite formation, as they are intrinsically higher due to the nanosize of both particles, at least at short time points. Therefore, the slight delay on apatite quality at day 1, might be attributed to the increasing Sr content that can slow the bioactive behavior of BGNPsSr, because of the inhibitory effect of Sr on the mineralization kinetics.[35] According to the classic apatite formation mechanism on bioactive glasses, the release and absorption of Ca from SBF onto the electronegative Si-OH groups, formed by hydrolysis of silicate network, attracts PO_4^{3-} from SBF to create nucleation sites.[36] Therefore, the released Sr into solution might interfere with apatite development by competitively binding to PO_4^{3-} compared to Ca. This observation agrees with previous studies showing the formation of carbonated bone-like hydroxyapatite after a similar reaction time of immersion in SBF.[35]

FTIR measurements monitored the apatite formation on the surface of the nanoparticles. The soaked samples also showed the characteristic Si-O-Si bending and stretching vibrations at 460, 810 and 1100 cm^{-1}, consistent with the silica network present on bioactive glasses (**Figure 2F**). After 7 days, the samples exhibited a vibration band at 1080 cm^{-1} and a double peak at 607 and 570 cm^{-1}, due to the stretching vibration of phosphate groups. After 7 days in SBF, the amorphous band (around 600 cm^{-1}) evolves into double peak (607 and 570 cm^{-1}), due to the stretching vibration of phosphate groups. The formation of the P-O dual band can be a bioactivity marker considered as first evidence of the appearance of crystalline carbonated bone-like hydroxyapatite.[37] These results indicated that the produced nanoparticles induced the growth of hydroxyapatite on their surface.

The quality of apatite formation on top of the BGNPs was also followed using XRD. The apatite formed after 3 and 7 days resembling the typical semi-crystalline hydroxyapatite

diffractogram at 2θ = 25.9°, 29°, 31.8°, 32.2°, 32.9°, 34°, 39.8°, 46.7°, 49.5°, 50.5° and 53.1° (**Figure 2G**).[27]

The quantitative analysis of the ions during and after SBF immersion was performed to understand the dissolution kinetics of the nanoparticles (**Figure 2H** and **Figure S5**). The concentrations of both Ca and P decreased as they were consumed for the formation of the apatite bone-like on the nanoparticles surface consistent with EDS results (**Table S4** and **Table S5**). The concentrations of Si ions were increased and then stagnated in the SBF solution. This may be due to the release of ions, loss of soluble SiO_2 from the surface of the glass specimens to the SBF solution, condensation, and re-polymerization of the SiO_2-rich layer. Calcium and phosphorous concentrations then dropped in the SBF solution increasing the silicon ion concentration after 7 days, and this may be due to the formation of an amorphous CaO-P_2O_5 layer on the surface of the glass sample.[38]

Overall, our results indicated that Sr incorporation does not critically influence the mineralization capability of the produced nanoparticles. These results confirm not only the expected bioactive nature of the nanoparticles but also the osteoconductive capacity of the newly developed BGNPsSr.

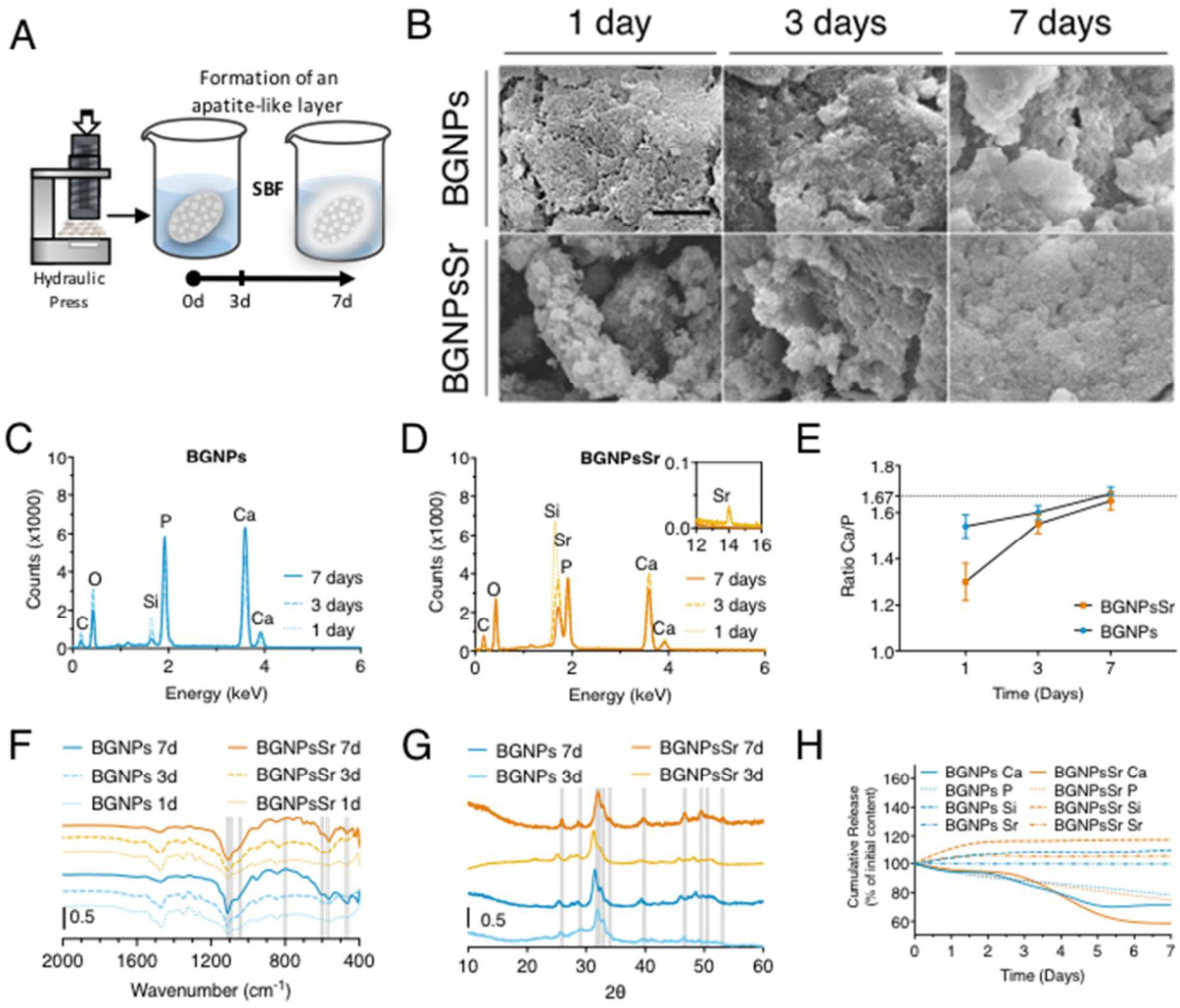

Figure 2. The bioactive behavior of the produced nanoparticles. **A)** Schematic representation of the *in vitro* bioactivity assessment. **B)** Representative SEM micrographs of BGNPs and BGNPsSr soaked in SBF solution during 1, 3 and 7 days. Scale Bar = 5 µm. SEM micrographs before soaking in SBF (0days) are present in **Figure S4A. C)** Identification of chemical elements using EDS after immersion of BGNPs in SBF for 1, 3, and 7 days. **D)** Identification of chemical elements using EDS after immersion of BGNPsSr in SBF for 1, 3, and 7 days. **E)** Ca/P ratio during 1, 3 and 7 days of immersion in SBF. **F)** FTIR spectra of the apatite formation on the surface of the nanoparticles. **G)** XRD (X-ray diffraction) spectra obtained for BGNPs after the

immersion in SBF (3 and 7 days). The principal characteristic hydroxyapatite peaks are indicated. The spectra obtained for BGNPs before the immersion in SBF (0 days) are depicted in **Figure S4B**. **H)** ICP (inductively coupled plasma) analyses of the evolution of Ca, Si and Sr in the SBF.

BIOCOMPATIBILITY ASSESSMENT OF THE BIOACTIVE GLASS NANOPARTICLES

In therapy scenario, biomaterials must not cause toxicity to the cells involved in bone regeneration. Along with new bone production, the development of vascularization is necessary to provide oxygen, nutrients, and growth factors essential to cell survival, integration and successful regeneration. This relation is referred as angiogenic-osteogenic coupling.[39] Recent investigations demonstrated that bioactive glasses not merely enhance bone formation but could stimulate angiogenesis,[40] and Sr ions proved advantageous.[41] Therefore, a preliminary biological response of the produced nanoparticles was studied in agglomerated discs using two well-characterized cells lines, SaOS-2 and HUVECs (**Figure 3A**).

The metabolic activity was evaluated using the Alamar blue assay that relies on the cytoplasmic reduction potential of metabolically viable cells. A significant increase in the metabolism was observed up to 7 days of culture for SaOS-2, while no significant impact on metabolic activity was observed for HUVECs, after seeding on the agglomerated nanoparticles (**Figure 3B**). The results also showed an increase in the metabolic activity with the time in culture for both cells lines, regardless of the particles. These findings denote that the produced nanoparticles do not negatively interfere with cell metabolism.

Figure 3C shows that cells were evenly distributed over the surface of the agglomerated nanoparticles after 1, 3 and 7 days of culture. After 1 day of culture, the nanoparticles sustained cell attachment, though no statistical significance was found in cell proliferation from 3 to 7 days (**Figure 3D**). Both nanoparticles formulations did not influence the spreading of SaOS-2 (**Figure 3E**). However, both nanoparticles favored the spread of HUVECs in the end of the study period. Images were also processed with a specific software for angiogenesis analysis which can detect pseudo-vascular organization of endothelial cells (see figure S7). The results not only demonstrated that the nano-nature of the nanoparticles could enhance cell anchorage and spread, but also that strontium elicits a positive effect on the behavior of angiogenic cells. Interestingly, the BGNPsSr seemed to enhance the response of HUVECs as a rearrangement of cell distribution that could be associated to an eventual tubular structure formation that was observed after 7 days of culture (**Figure 3C** and **Figure S7**). This morphology could be an indication of the effect of strontium ions in the angiogenesis process ($P<0.03$ in the angiogenic descriptors, **Table S6**). This microvascular behavior has been similarly reported for ceramics containing strontium, where the ionic release played a corporative role in stimulating endothelial functions.[42]

Besides the positive effect of BGNPsSr on the HUVECs morphology, these results also showed an absence of cytotoxicity of the nanoparticles, reinforcing their appropriateness in tissue engineering applications.

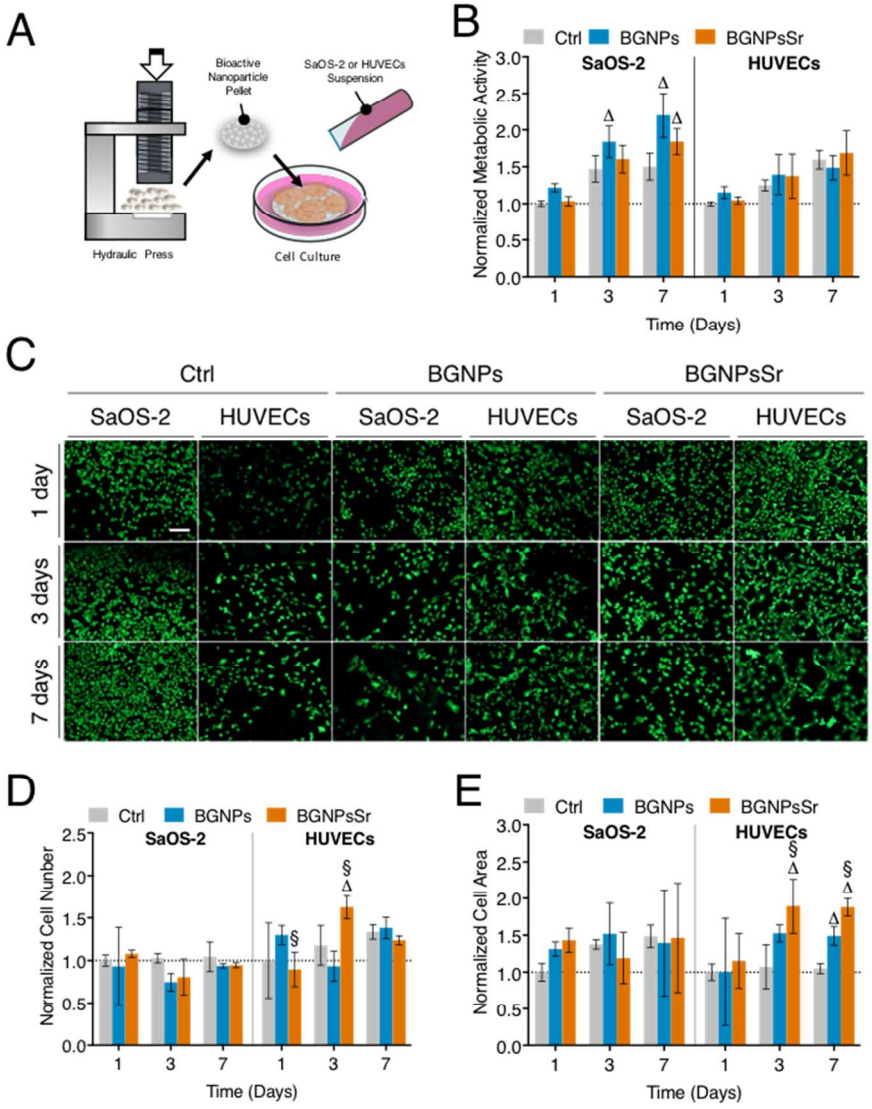

Figure 3. Biocompatibility assessment. **A)** Schematic representation of the *in vitro* cell biocompatibility studies. **B)** Alamar blue assay results. **C)** Representative photographs of calcein−AM staining of SaOS-2 and HUVECs during the cell culture time (scale bar = 200 µm). **D)** Cell number of SaOS-2 and HUVECs cells seeded on BGNPs and BGNPsSr agglomerated samples based on an automated analysis where each particle was detected as an object representing a cell. **E)** Cell area of SaOS-2 and HUVECs cells seeded on BGNPs and BGNPsSr

agglomerates based on automated measurement features and analyzed after image processing (**Figure S6**). The data were normalized to the control at first time point for each cell type line. When applicable, (Δ) depicts a positive statistical difference when compared with the control at each time point (nanoparticles effect), while (§) shows the statistical difference of BGNPsSr when compared with BGNPs (strontium effect).

GENE AND PROTEIN EXPRESSION TOWARDS OSTEOGENIC COMMITMENT

The combination of biomaterials with stem cells has demonstrated to improve bone healing. Stem cells could show a temporal development similar to *in vivo* bone formation.[43] Therefore, and considering the previous results, it becomes crucial to evaluate whether the nanoparticles could drive osteogenic differentiation to understand their physiological outcome. The cellular effect of strontium nanoscaled bioactive glasses has been reported in the literature (**Table S7**). However, studies on the effect of strontium doped bioactive glass nanoparticles in stem cells are still required. The osteogenic potential of the produced nanoparticles was examined on stem cells derived from adipose tissue (**Figure 4A**). These cells were chosen as the stem cell source due to its abundance, easy access, nonimmunogenicity, and as it represents a suitable cell type for clinical translation into musculoskeletal regeneration treatments.[44] In this study, the nanoparticles were supplemented in the cell culture medium as a well-dispersed form.

Osteogenic differentiation is a gradual process, characterized by developmental stages, in which alterations in this defined sequence can induce or inhibit differentiation and so bone formation.[45] Therefore, this temporal pattern was assessed by real-time PCR regarding the expression of main osteogenic differentiation genes analyzed at 7, 14, and 21 days. Runt-related transcription factor 2 (*RUNX2)* affects osteogenic differentiation in the early stages and is considered a key integrator in the signaling cascade as it induces other downstream osteo-related genes such as type I collagen, osteocalcin (*OCN*), and secreted phosphoprotein 1 (*SPP1*).[46] The nanoparticles influenced the expression levels of *RUNX2* in the initial culture periods, in which, a significant upregulation of *RUNX2* occurred at 7 days for all the cultures media. A relationship with BGNPsSr only appears in the basal and osteogenic medium at 7 days, where the levels were

similar to the control in osteogenic medium (**Figure 4B**). Also, the extent of *RUNX2* expression correlated with the expression of type I collagen, *OCN*, and *SPP1* ($P<0.03$, **Table S14**). Collagen type I alpha 1 (*COL1A1*) is expressed in the first periods and downregulated in the succeeding osteoblast differentiation, being necessary for the progress of the bone cell phenotype.[46] The results showed upregulation of *COL1A1* expression at 7 days for the hASCs cultured in osteogenic medium and when cells were cultured with BGNPsSr despite the culture medium (**Figure 4C**). This finding denotes that the upregulation levels on the basal and osteoinductive media are similar to the ones ascribed to the osteogenic medium when strontium is present. Moreover, the BGNPsSr possess higher upregulations levels than BGNPs. Alkaline phosphatase (ALP) is a membrane-bound enzyme linked with osteogenic differentiation and phosphate metabolism.[47] The results showed that both nanoparticles induced an upregulation of *ALPL* gene in the initial 7 days in all culture media (**Figure 4D**). These findings remain consistent with reports that demonstrated reduced levels of *ALPL* in late-stage cultures.[47] This result suggested that the nanoparticles could enhance the *ALPL* activity of hASCs absent osteogenic supplements. Osterix (*OSX)* is an osteoblast transcription factor essential for osteoblast differentiation and bone formation (*OSX* knock-out mice lack bone completely).[48] *OSX* expression was enhanced at 7 days in osteogenic medium and remained similar in the following time points for all media. However, an upregulation was found for BGNPsSr in basal and osteoinductive media (**Figure 4E**). Studies have reported that only differentiated osteoblasts could express osteocalcin (*OCN)*.[49] Herein, the results showed that only the BGNPsSr upregulated the *OCN* expression at 7 days in all culture media (**Figure 4F**). *SPP1* expression increased at 7 days in the presence of both nanoparticles but was only enhanced in osteogenic medium (**Figure 4G**).

Altogether, the upregulation of osteogenic differentiation genes were increased by both types of nanoparticles. However, only the BGNPsSr was capable of significantly upregulating all the selected genes in complete basal conditions. These findings indicate that the BGNPsSr are a strong inducer of stem cells through osteocommmitment, even without osteogenic supplementation. In this regard, the mechanism of strontium on bone formation was reported to involve the Ras/MAPK signaling pathway and the downstream transcription factor *RUNX2*.[50]

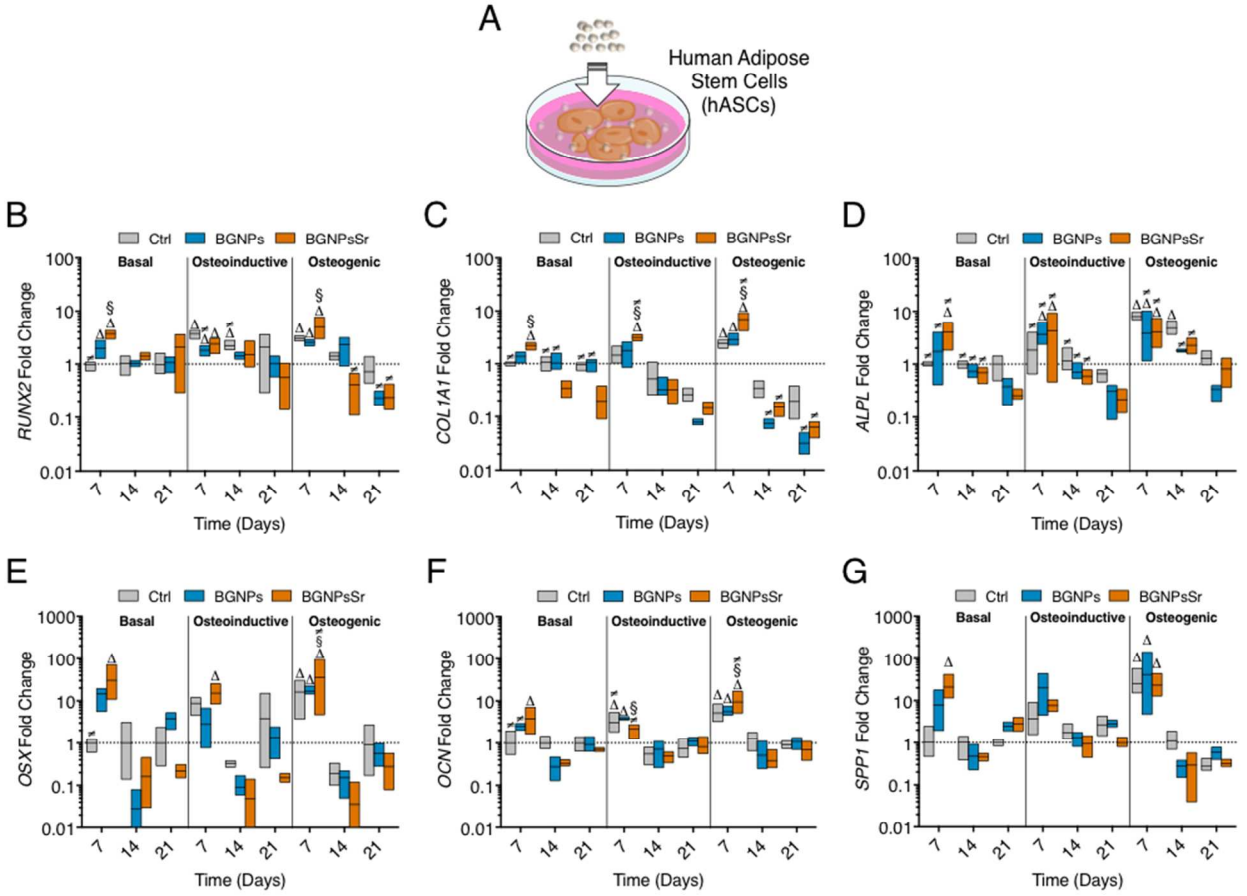

Figure 4. Analysis of the gene expression for early osteogenic commitment. **A)** Schematic representation of the cell culture methodology. **B)** Runt-related transcription factor 2 (*RUNX2*) gene expression. The statistical analysis is represented in **Table S8**. **C)** Collagen type I

(COL1A1) gene expression. The statistical analysis is represented in **Table S9**. **D)** Alkaline phosphatase (*ALPL*) gene expression. The statistical analysis is represented in **Table S10**. **E)** Osterix (*OSX*) gene expression. The statistical analysis is represented in **Table S11**. **F)** Osteocalcin (*OCN*) gene expression. The statistical analysis is represented in **Table S12**. **G)** Secreted phosphoprotein 1 (*SPP1*) gene expression. The statistical analysis is represented in **Table S13**. When applicable, (Δ) depicts statistical upregulation when compared with the control in basal media at each time point (nanoparticles effect); (§) shows the statistical difference of BGNPsSr when compared with BGNPs (strontium effect), while (≠) denotes a statistical difference when compared with the control with osteogenic media at each time point (media effect).

The cell metabolic activity (indirectly related to cell viability), and proliferation are relevant parameters in cell response. The MTS assay was used to assess cell metabolism relying on the mitochondrial activity of hASCs.[51] Both nanoparticles supplemented in the cell culture medium did not affect hASCs metabolic activity (**Figure 5A**). The spreading of hASCs in the presence of nanoparticles denotes their stem cell biocompatibility. The osteogenic control had a significantly higher metabolic activity than both nanoparticles, which could be due to the higher differentiation of hASCs in the presence of both nanoparticles. Similar phenomena have been previously reported.[52] Clusters of nanoparticles were also observed inside and on the outer surface of the plasma membrane of hASCs (**Figure S8**), engulfed by membrane protrusions which might indicate endocytosis (**Figure 5B**).

The osteogenic differentiation of hASCs in the presence of particles was also evaluated at the protein level. The expression of bone-specific proteins, osteocalcin (OCN) and osteopontin (OPN), were evaluated by immunofluorescence at 14 and 21 days in either basal or osteogenic media (**Figure 5C** and **D**). The osteoinductive medium was eliminated from this study since the previous results showed no relevant effect on cell behavior (**Table S14**). OCN is an early marker of osteogenic differentiation and reported as an osteoblast-specific ECM phosphoprotein known to be involved in cell attachment, proliferation, and in the onset of matrix deposition.[53] OPN is a non-collagenous protein of the bone extracellular matrix (ECM) and is produced by osteoblasts involved in endochondral ossification.[54] The osteogenic markers OCN and OPN were detected in all conditions, and a high protein expression up to day 14 shows bone ECM maturation (**Figure 5E** and **F**).[55]

Overall, the upregulation of genes and the synthesis of the selected proteins were increased by both nanoparticles without requiring osteogenic supplements. These findings further suggest that the particles and their dissolution products are likely influencing the commitment of hASCs toward osteoblast differentiation. It is hypothesized that ions released from the nanoparticles may exert an osteogenic effect by locally modifying the culture medium. The presence of BGNPsSr was also associated with higher stimulation of both early and late osteoblast markers at the gene and protein levels in comparison with BGNPs. These observations demonstrated the hASCs commitment towards osteoblast differentiation for all culture conditions.

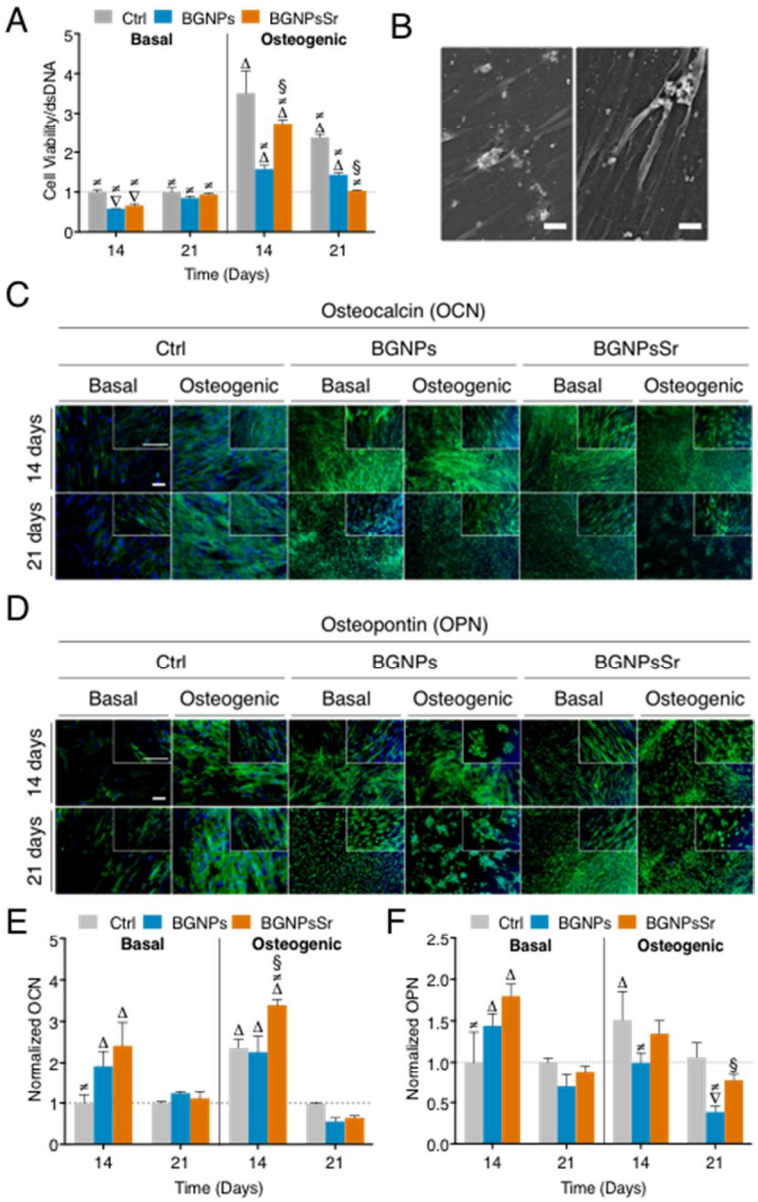

Figure 5. Analysis of the protein expression for early osteogenic commitment. **A)** Cell viability of hASCs cells exposed BGNPs and BGNPsSr subtracted from the positive control (cells cultured in nanoparticles-free media). The statistical analysis is represented in **Table S15**. **B)** Scanning electron microscopic analysis of hASCs in the presence of both nanoparticles after 14 days in culture, showing the bound cell layer covering part of the bioactive glass particle

surface and the cell attached to the substrate throught cytoplasmic digitations. Scale bar = 10 μm. **C)** Immunofluorescence of osteocalcin for hASCs cultured with BGNPs and BGNPs-Sr, after 14 and 21 days in culture. Scale bar = 10 μm. **D)** Immunofluorescence of osteopontin for hASCs cultured with BGNPs and BGNPs-Sr, after 14 and 21 days in culture. Scale bar = 100 μm. **E)** Quantification of osteocalcin through image analysis. The statistical analysis is represented in **Table S16**. **F)** Quantification of osteopontin through image analysis. The statistical analysis is represented in **Table S17**. When applicable, (Δ) depicts statistical upregulation and (∇) depicts statistical downregulation, when compared with the control in basal media at each time point (nanoparticles effect); (§) shows the statistical difference of BGNPsSr when compared with BGNPs (strontium effect), while (≠) denotes a statistical difference when compared with the control in osteogenic media at each time point (media effect).

CONCLUSIONS

In this study, we have demonstrated the biological performance of bioactive glass nanoparticles for osteogenic applications in bone tissue engineering. New nanoparticles doped with strontium ions have been successfully developed, and a comprehensive characterization for regenerative medicine was performed. The produced nanoparticles - BGNPs and BGNPsSr - presented a bioactive behavior, leading to the formation of an apatite layer on the surface when immersed in SBF. Moreover, HUVECs, SaOS-2 and, hASCs kept their viability levels in the presence of both nanoparticles in comparison with cells not exposed to the particles. The BGNPsSr formulation promoted the angiogenic phenotype of HUVECs. To investigate the ion release effect of BGNPs and BGNPsSr on osteoblast differentiation of hASCs, the gene and proteins expression of early and late osteoblast markers were examined. Overall, the biochemical data showed that the selected genes and proteins were typically expressed throughout the culture period indicating that both nanoparticles represent an adequate support for osteogenic differentiation. The results also show that the partial substitution of Ca for Sr in the nanoparticles is effective on favoring the expression of genes and proteins, indicating these nanoparticles could govern stem cells through osteocommitment, even without osteogenic supplementation. Therefore, the developed BGNPsSr may be used as biological agents to modulate the behavior of stem cells. These findings open new possibilities for BGNPsSr alone or as additives in a matrix (e.g., scaffolds or hydrogels) avoiding the need of culturing stem cells with typical osteogenic cocktails in cell culture or during the *in vivo* implantation. Therefore, incorporating Sr into BGNPs can be used to design a new generation of (i) bioactive nanocomposites or (ii) cell

internalizable ingredient in "scaffold-free" strategies for stem cell modulation in vascularized bone-engineered applications.

METHODS

Bioactive glass nanoparticles preparation: The preparation of the ternary form of BGNPs followed a described protocol comprising sequential reagent dissolutions that resulted in hydrolysis and polycondensation reactions (**Information S1**).[27] A similar procedure was followed to obtain Sr-doped BGNPs (BGNPsSr), but in this case, the sol-gel precursor solution contained strontium nitrate (Sigma-Aldrich, see **Table S2**).

In vitro bioactivity study: The tests were carried out for 1, 3 and 7 days at 37 °C in disc shape agglomerates. Discs of both BGNPs and BGNPsSr, with an approximate weight of 100 mg and ø 4 mm, were produced through a compact and inexpensive hand-driven press (MHP-1, Shimadzu; Germany), ensuring the reproducibility of the operation. The samples were immersed in 30 mL of simulated body fluid (SBF, **Table S3**) under shaking (30 rpm). After removing the samples from SBF, they were rinsed with distilled water, dried at 60 °C for 24 h and kept in desiccators. The preparation of SBF followed the protocol described by Kokubo and Takadama.[33]

Elemental and morphological assessment: The nanoparticles were dispersed in 100% ethanol and fixed by mutual conductive adhesive tape. Energy dispersive spectroscopy (EDS; QUANTAX200 Bruker, Germany) was first performed to analyze the elemental composition of the nanoparticles. A scanning electron microscope (SEM; JSM-6010LV, JEOL, Japan), operated at 15 kV, was used to study the morphology of the nanoparticles produced. Before SEM acquisition, all samples were coated with a thin layer of carbon using a sputter coater (EM

ACE600, Leica, Germany). Images were taken after short exposure times to ensure no beam damage to the nanoparticles during analysis.

Size distribution: Nanoparticles solutions were prepared at 1 mg mL^{-1} in ethanol, followed by 5 min of ultrasonication, and then examined under dynamic light scattering (DLS, Malvern instrument 2000) at 25 ºC, setting a minimum of 10 and a maximum of 100 runs per measurement. The measurements were performed in triplicate.

Fourier-Transformed Infrared (FTIR) spectroscopy analysis: The samples were dried at room temperature and combined with potassium bromide (KBr), producing discs. Then the infrared spectra were recorded using an FTIR Spectrometer (IRPrestige-21, Shimadzu; Germany) in the wavelength range of 4400-400 cm^{-1}, as an average of 32 scans.

Measurement of element concentrations in SBF: SBF solutions from the in vitro bioactivity study, collected at each time point, were filtered (0.22 μm), diluted (1:10) in 1% nitric acid (HNO3) and kept at -20 °C. The levels of calcium, phosphorous, silicon, and strontium were measured by inductively coupled plasma optical emission spectroscopy (ICP-OES; JY2000-2, Jobin Yvon, Horiba) against standard solutions. At least five samples were used per condition and per time point.

X-ray diffraction (XRD) spectra of the nanoparticles: X-ray diffraction (XRD) spectra were collected on a Philips PW1700 Series automated powder diffractometer using Cu Ka radiation operated at 40 kV and 40 mA. Data were collected between 5° and 80° 2θ with a step of 0.04° 2θ and a dwell time of 1.5 s.

Cytotoxicity screening: A human osteosarcoma osteoblast-like cell line (SaOS-2, ATCC) and human umbilical vein endothelial cell line (HUVECs, Alfagene) were used as well-established

cell lines for preliminary cytocompatibility studies. To investigate any pH changes caused by BGNPs, as has been reported in the literature,[30] the agglomerated discs samples of BGNPs or BGNPsSr (produced as described in the in vitro bioactivity study - Section 3.2) were rinsed with sterile PBS for 24 h. As no significant change in pH was detected over the study period (**Figure S9**), the agglomerated discs samples were used for cell culture purposes right after preparation. The labeling of live cells, the cytoplasm staining, and the metabolic activity protocol is detailed in **Information S2**. For quantification of cell number and cell area, all images were processed using algorithms developed in ImageJ (version 2.0, NIH, USA) and by using specific routines written by the authors. Briefly, image stacks in the green channel were used as input, and then thresholded, segmented, and measured by features established in the software. Six images per condition were used.

Osteogenic Differentiation: Human adipose stem cells (hASCs) were cultured with bioactive glass nanoparticles dispersed in the medium with and without osteogenic supplements. After isolation and expansion (**Information S3**), the cells could adhere for 24 h, and the basal medium was replaced with osteoconductive, or osteogenic medium, either containing a dispersion of BGNPs or BGNPsSr at 100 $\mu g\,mL^{-1}$, as higher doses showed to reduce cell viability and proliferation.[56] For that, sterilized nanoparticles (dry heat at 180 °C for 2 h) were dispersed in an ultrasonic bath in α-MEM medium (with no supplementation) for 5 min, autoclaved, and then supplemented as the basal medium. The osteogenic medium consisted in the basal medium supplemented with 10 mM beta-glycerophosphate (Sigma-Aldrich), 10-8 mM dexamethasone (Sigma-Aldrich), and 50 $mg\,mL^{-1}$ l-ascorbic acid 2-phosphate sesquimagnesium salt hydrate (Sigma-Aldrich). The osteoconductive medium was similar to osteogenic medium but without

dexamethasone supplementation. Cells were then incubated in a humidified environment at 37 °C with 5% CO2 for 7, 14 and 21 days. The upper half of the culture medium was renewed every 3 days to ensure nanoparticles remaining at the bottom of the wells. Cells cultured in basal, osteogenic and osteoconductive media absent nanoparticles were experimental controls (Ctrl).

Real-time reverse transcriptase-polymerase chain reaction (RT-PCR): Total RNA was extracted using TRI Reagent (Sigma-Aldrich), following the manufacturer instructions. RNA quantity and purity were assessed with a NanoDrop ND-1000 Spectrophotometer (NanoDrop Technologies, USA). First-strand complementary DNA (cDNA) synthesis was performed using qScript™ cDNA synthesis Kit (Quanta Biosciences) on a Mastercycler ep realplex thermal cycler (Eppendorf, USA), using 1 μg of RNA.

The quantification of the transcripts of the genes of interest was carried out by RT-PCR in a real-time Mastercycler® ep realplex gradient S machine (Eppendorf, USA) using PerfeCTA™ SYBR® Green FastMix kit (Quanta Biosciences) following the manufacturer's protocol. The primers were designed using the Primer 3 online software (v0.4.0, Whitehead Institute, USA) and synthesized by MGW Biotech (Germany). The primers sequences and annealing temperatures for bone-specific genes, collagen type I (*COL1A1*), alkaline phosphatase (*ALPL*), runt-related transcription factor 2 (*RUNX2*), secreted phosphoprotein 1 (*SPP1*), osteocalcin (*OCN*), osterix (*OSX*), and glyceraldehyde-3-phosphate dehydrogenase (*GAPDH*) are depicted in **Table S18**. The relative quantification of the target genes was performed using the Livak method.[57] For each sample, the transcripts expression data were normalized to *GAPDH*, used as the housekeeping gene, and were expressed as fold changes relative to the expression of hASCs

cultured in basal, osteogenic or osteoconductive medium absent bioactive glass nanoparticles (Ctrl).

Cell number and metabolic activity: The quantity of double strained DNA (dsDNA) that is directly proportional to the cell number was determined using a fluorometric dsDNA quantification kit (PicoGreen, Molecular Probes, Invitrogen), according to the manufacturer's instructions. The effect of the nanoparticles on metabolic activity of hASCs was also investigated through MTS assay. The detailed protocol is described in **Information S4**.

Expression of proteins associated with the osteogenic process: Immunolabelling against osteopontin (OPN, ab14175) and osteocalcin (OCN, ab13418) was performed after 14 and 21 days of culture. A detailed protocol can be found in **Information S5**.

Statistical analysis: Each experiment was performed with, at least, three independent triplicates. First, a Shapiro-Wilk test was used to ascertain the data normality. The results indicated that non-parametric test should be employed for all comparisons. Results are presented as mean ± standard deviation when applicable. Statistical analysis was performed ANOVA with post hoc Tukey's or Sidak's multiple comparisons tests, using GraphPad Prism v7.00 software (San Diego, USA). Statistical significance was set at a p-value of ≤ 0.0332 (*); ≤ 0.0021 (**); ≤ 0.0002 (***); or ≤ 0.0001 (****).

ASSOCIATED CONTENT

Supporting Information: The following files are available free of charge.

Supplementary_Information - .docx file containing supplementary figures, tables, and descriptions.

AUTHOR INFORMATION

Corresponding Author

*Correspondence should be addressed to João F. Mano (jmano@ua.pt)

Present Addresses

João F. Mano present address: Department of Chemistry, CICECO – Aveiro Institute of Materials, University of Aveiro, 3810-193 Aveiro, Portugal. E-mail: jmano@ua.pt

Author Contributions

The manuscript was written through contributions of all authors and all authors have given approval to the final version.

ACKNOWLEDGMENT

This work was supported by the Portuguese Foundation for Science and Technology Foundation (FCT) through the doctoral grant SFRH/BD/73174/2010 of Álvaro Leite and FCT and Fundo Social Europeu através do Programa Operacional do Capital Humano (FSE/POCH), PD/59/2013, for the doctoral grant PD/BD/113802/2015 of Ana Gonçalves.

REFERENCES

(1) Luz, G. M.; Mano, J. F. Chitosan/bioactive glass nanoparticles composites for biomedical applications. *Biomedical Materials* **2012**, *7*, 054104.

(2) Leite, A. J.; Mano, J. F. Biomedical applications of natural-based polymers combined with bioactive glass nanoparticles. *Journal of Materials Chemistry B* **2017**, *5*, 4555-4568.

(3) Jones, J. R. Review of bioactive glass: From Hench to hybrids. *Acta Biomaterialia* **2013**, *9*, 4457-4486.

(4) Xynos, I. D.; Hukkanen, M. V. J.; Batten, J. J.; Buttery, L. D.; Hench, L. L.; Polak, J. M. Bioglass (R) 45S5 stimulates osteoblast turnover and enhances bone formation in vitro: Implications and applications for bone tissue engineering. *Calcified Tissue International* **2000**, *67*, 321-329.

(5) Kokubo, T. Bioactive glass ceramics: properties and applications. *Biomaterials* **1991**, *12*, 155-163.

(6) Luz, G. M.; Mano, J. F. Biomimetic design of materials and biomaterials inspired by the structure of nacre. *Philosophical Transactions of the Royal Society A: Mathematical, Physical and Engineering Sciences* **2009**, *367*, 1587-1605.

(7) Jiang, W.; Kim, B. Y. S.; Rutka, J. T.; Chan, W. C. W. Nanoparticle-mediated cellular response is size-dependent. **2008**, *3*, 145.

(8) Wei, G.; Ma, P. X. Nanostructured Biomaterials for Regeneration. *Advanced Functional Materials* **2008**, *18*, 3566-3582.

(9) Alves, N. M.; Pashkuleva, I.; Reis, R. L.; Mano, J. F. Controlling Cell Behavior Through the Design of Polymer Surfaces. *Small* **2010**, *6*, 2208-2220.

(10) Zhang, L.; Webster, T. J. Nanotechnology and nanomaterials: Promises for improved tissue regeneration. *Nano Today* **2009**, *4*, 66-80.

(11) Webster, T. J.; Ergun, C.; Doremus, R. H.; Siegel, R. W.; Bizios, R. Enhanced functions of osteoblasts on nanophase ceramics. *Biomaterials* **2000**, *21*, 1803-1810.

(12) Luz, G. M.; Mano, J. F. A nanotectonics approach to produce hierarchically organized bioactive glass nanoparticles-based macrospheres. *Nanoscale* **2012**, *4*, 6293-6297.

(13) Alves, N. M.; Leonor, I. B.; Azevedo, H. S.; Reis, R. L.; Mano, J. F. Designing biomaterials based on biomineralization of bone. *Journal of Materials Chemistry* **2010**, *20*, 2911-2921.

(14) Misra, S. K.; Mohn, D.; Brunner, T. J.; Stark, W. J.; Philip, S. E.; Roy, I.; Salih, V.; Knowles, J. C.; Boccaccini, A. R. Comparison of nanoscale and microscale bioactive glass on the properties of P(3HB)/Bioglass® composites. *Biomaterials* **2008**, *29*, 1750-1761.

(15) Kim, J.-J.; El-Fiqi, A.; Kim, H.-W. Synergetic Cues of Bioactive Nanoparticles and Nanofibrous Structure in Bone Scaffolds to Stimulate Osteogenesis and Angiogenesis. *ACS Applied Materials & Interfaces* **2017**, *9*, 2059-2073.

(16) Vichery, C.; Nedelec, J.-M. Bioactive Glass Nanoparticles: From Synthesis to Materials Design for Biomedical Applications. *Materials* **2016**, *9*.

(17) Zheng, K.; Boccaccini, A. R. Sol-gel processing of bioactive glass nanoparticles: A review. *Advances in Colloid and Interface Science* **2017**, *249*, 363-373.

(18) Hoppe, A.; Güldal, N. S.; Boccaccini, A. R. A review of the biological response to ionic dissolution products from bioactive glasses and glass-ceramics. *Biomaterials* **2011**, *32*, 2757-2774.

(19) Govindaraj, D.; Rajan, M.; Munusamy, M. A.; Alarfaj, A. A.; Sadasivuni, K. K.; Kumar, S. S. The synthesis, characterization and in vivo study of mineral substituted hydroxyapatite for prospective bone tissue rejuvenation applications. *Nanomedicine: Nanotechnology, Biology and Medicine* **2017**, *13*, 2661-2669.

(20) Pors Nielsen, S. The biological role of strontium. *Bone* **2004**, *35*, 583-588.

(21) Jensen, J.; Stang, H.; Kringsholm, B.; Pritzl, G.; Sørensen, O. Relationship between trace element content and mechanical bone strength. *Bone* **1997**, *20*, 104.

(22) Meunier , P. J.; Roux , C.; Seeman , E.; Ortolani , S.; Badurski , J. E.; Spector , T. D.; Cannata , J.; Balogh , A.; Lemmel , E.-M.; Pors-Nielsen , S.; Rizzoli , R.; Genant , H. K.; Reginster , J.-Y. The Effects of Strontium Ranelate on the Risk of Vertebral Fracture in Women with Postmenopausal Osteoporosis. *New England Journal of Medicine* **2004**, *350*, 459-468.

(23) Wu, C.; Zhou, Y.; Lin, C.; Chang, J.; Xiao, Y. Strontium-containing mesoporous bioactive glass scaffolds with improved osteogenic/cementogenic differentiation of periodontal ligament cells for periodontal tissue engineering. *Acta Biomaterialia* **2012**, *8*, 3805-3815.

(24) Santocildes-Romero, M. E.; Crawford, A.; Hatton, P. V.; Goodchild, R. L.; Reaney, I. M.; Miller, C. A. The osteogenic response of mesenchymal stromal cells to strontium-substituted bioactive glasses. *Journal of Tissue Engineering and Regenerative Medicine* **2015**, *9*, 619-631.

(25) Autefage, H.; Gentleman, E.; Littmann, E.; Hedegaard, M. A. B.; Von Erlach, T.; O'Donnell, M.; Burden, F. R.; Winkler, D. A.; Stevens, M. M. Sparse feature selection methods identify unexpected global cellular response to strontium-containing materials. *Proc. Natl. Acad. Sci. U. S. A.* **2015**, *112*, 4280-4285.

(26) Strobel, L. A.; Hild, N.; Mohn, D.; Stark, W. J.; Hoppe, A.; Gbureck, U.; Horch, R. E.; Kneser, U.; Boccaccini, A. R. Novel strontium-doped bioactive glass nanoparticles enhance proliferation and osteogenic differentiation of human bone marrow stromal cells. *Journal of Nanoparticle Research* **2013**, *15*, 1-9.

(27) Luz, G. M.; Mano, J. F. Preparation and characterization of bioactive glass nanoparticles prepared by sol-gel for biomedical applications. *Nanotechnology* **2011**, *22*, 494014.

(28) Leite, A. J.; Sarker, B.; Zehnder, T.; Silva, R.; Mano, J. F.; Boccaccini, A. R. Bioplotting of a bioactive alginate dialdehyde-gelatin composite hydrogel containing bioactive glass nanoparticles. *Biofabrication* **2016**, *8*, 035005.

(29) Fredholm, Y. C.; Karpukhina, N.; Law, R. V.; Hill, R. G. Strontium containing bioactive glasses: Glass structure and physical properties. *Journal of Non-Crystalline Solids* **2010**, *356*, 2546-2551.

(30) Naruphontjirakul, P.; Greasley Sarah, L.; Chen, S.; Porter Alexandra, E.; Jones Julian, R. Monodispersed strontium containing bioactive glass nanoparticles and MC3T3-E1 cellular response. In *Biomedical glasses*; 2016; pp 72–81.

(31) O'Donnell, M. D.; Hill, R. G. Influence of strontium and the importance of glass chemistry and structure when designing bioactive glasses for bone regeneration. *Acta Biomaterialia* **2010**, *6*, 2382-2385.

(32) Song, W.; Veiga, D. D.; Custódio, C. A.; Mano, J. F. Bioinspired Degradable Substrates with Extreme Wettability Properties. *Advanced Materials* **2009**, *21*, 1830-1834.

(33) Kokubo, T.; Takadama, H. How useful is SBF in predicting in vivo bone bioactivity? *Biomaterials* **2006**, *27*, 2907-2915.

(34) Leite, A. J.; Caridade, S. G.; Mano, J. F. Synthesis and characterization of bioactive biodegradable chitosan composite spheres with shape memory capability. *Journal of Non-Crystalline Solids* **2016**, *432, Part A*, 158-166.

(35) Hoppe, A.; Sarker, B.; Detsch, R.; Hild, N.; Mohn, D.; Stark, W. J.; Boccaccini, A. R. In vitro reactivity of Sr-containing bioactive glass (type 1393) nanoparticles. *Journal of Non-Crystalline Solids* **2014**, *387*, 41-46.

(36) Ohtsuki, C.; Kokubo, T.; Yamamuro, T. Mechanism of apatite formation on CaOSiO2P2O5 glasses in a simulated body fluid. *Journal of Non-Crystalline Solids* **1992**, *143*, 84-92.

(37) Koutsopoulos, S. Synthesis and characterization of hydroxyapatite crystals: A review study on the analytical methods. *Journal of Biomedical Materials Research* **2002**, *62*, 600-612.

(38) Oliveira, J. M.; Correia, R. N.; Fernandes, M. H. Effects of Si speciation on the in vitro bioactivity of glasses. *Biomaterials* **2002**, *23*, 371-379.

(39) Saran, U.; Gemini Piperni, S.; Chatterjee, S. Role of angiogenesis in bone repair. *Archives of Biochemistry and Biophysics* **2014**, *561*, 109-117.

(40) Miguez-Pacheco, V.; Gorustovich, A. A.; Boccaccini, A. R.; Roether, J. A. Bioactive Glasses for Soft Tissue Engineering Applications. In *Bioactive Glasses*; Royal Society of Chemistry: 2016; pp 336-361.

(41) Zhang, W.; Cao, H.; Zhang, X.; Li, G.; Chang, Q.; Zhao, J.; Qiao, Y.; Ding, X.; Yang, G.; Liu, X.; Jiang, X. A strontium-incorporated nanoporous titanium implant surface for rapid osseointegration. *Nanoscale* **2016**, *8*, 5291-5301.

(42) Wang, G.; Roohani-Esfahani, S.-I.; Zhang, W.; Lv, K.; Yang, G.; Ding, X.; Zou, D.; Cui, D.; zreiqat, H.; Jiang, X. Effects of Sr-HT-Gahnite on osteogenesis and angiogenesis by adipose derived stem cells for critical-sized calvarial defect repair. *Scientific Reports* **2017**, *7*, 41135.

(43) Jin, Y.; Zhang, W.; Liu, Y.; Zhang, M.; Xu, L.; Wu, Q.; Zhang, X.; Zhu, Z.; Huang, Q.; Jiang, X. rhPDGF-BB Via ERK pathway osteogenesis and adipogenesis balancing in ADSCs for critical-sized calvarial defect repair. *Tissue Engineering Part A* **2014**, *20*, 3303-3313.

(44) Gimble, J. M.; Grayson, W.; Guilak, F.; Lopez, M. J.; Vunjak-Novakovic, G. Adipose tissue as a stem cell source for musculo-skeletal regeneration. *Frontiers in bioscience (Scholar edition)* **2011**, *3*, 69-81.

(45) Owen, T. A.; Aronow, M.; Shalhoub, V.; Barone, L. M.; Wilming, L.; Tassinari, M. S.; Kennedy, M. B.; Pockwinse, S.; Lian, J. B.; Stein, G. S. Progressive development of the rat osteoblast phenotype in vitro: Reciprocal relationships in expression of genes associated with osteoblast proliferation and differentiation during formation of the bone extracellular matrix. *Journal of Cellular Physiology* **1990**, *143*, 420-430.

(46) Gaharwar, A. K.; Mihaila, S. M.; Swami, A.; Patel, A.; Sant, S.; Reis, R. L.; Marques, A. P.; Gomes, M. E.; Khademhosseini, A. Bioactive Silicate Nanoplatelets for Osteogenic Differentiation of Human Mesenchymal Stem Cells. *Advanced Materials* **2013**, *25*, 3329-3336.

(47) Golub, E. E.; Boesze-Battaglia, K. The role of alkaline phosphatase in mineralization. *Current Opinion in Orthopaedics* **2007**, *18*, 444-448.

(48) Nakashima, K.; Zhou, X.; Kunkel, G.; Zhang, Z.; Deng, J. M.; Behringer, R. R.; de Crombrugghe, B. The Novel Zinc Finger-Containing Transcription Factor Osterix Is Required for Osteoblast Differentiation and Bone Formation. *Cell* **2002**, *108*, 17-29.

(49) Chen, J.; Singh, K.; Mukherjee, B. B.; Sodek, J. Developmental Expression of Osteopontin (OPN) mRNA in Rat Tissues: Evidence for a Role for OPN in Bone Formation and Resorption. *Matrix* **1993**, *13*, 113-123.

(50) Peng, S.; Zhou, G.; Luk, K. D. K.; Cheung, K. M. C.; Li, Z.; Lam, W. M.; Zhou, Z.; Lu, W. W. Strontium Promotes Osteogenic Differentiation of Mesenchymal Stem Cells Through the Ras/MAPK Signaling Pathway. *Cellular Physiology and Biochemistry* **2009**, *23*, 165-174.

(51) Hamid, R.; Rotshteyn, Y.; Rabadi, L.; Parikh, R.; Bullock, P. Comparison of alamar blue and MTT assays for high through-put screening. *Toxicology in Vitro* **2004**, *18*, 703-710.

(52) Cadafalch Gazquez, G.; Chen, H.; Veldhuis, S. A.; Solmaz, A.; Mota, C.; Boukamp, B. A.; van Blitterswijk, C. A.; ten Elshof, J. E.; Moroni, L. Flexible Yttrium-Stabilized Zirconia Nanofibers Offer Bioactive Cues for Osteogenic Differentiation of Human Mesenchymal Stromal Cells. *ACS Nano* **2016**, *10*, 5789-5799.

(53) Nakamura, A.; Dohi, Y.; Akahane, M.; Ohgushi, H.; Nakajima, H.; Funaoka, H.; Takakura, Y. Osteocalcin Secretion as an Early Marker of In Vitro Osteogenic Differentiation of Rat Mesenchymal Stem Cells. *Tissue Engineering Part C: Methods* **2009**, *15*, 169-180.

(54) Denhardt, D. T.; Noda, M. Osteopontin expression and function: Role in bone remodeling. *Journal of Cellular Biochemistry* **1998**, *72*, 92-102.

(55) Mizuno, M.; Kuboki, Y. Osteoblast-Related Gene Expression of Bone Marrow Cells during the Osteoblastic Differentiation Induced by Type I Collagen. *The Journal of Biochemistry* **2001**, *129*, 133-138.

(56) Tsigkou, O.; Labbaf, S.; Stevens, M. M.; Porter, A. E.; Jones, J. R. Monodispersed Bioactive Glass Submicron Particles and Their Effect on Bone Marrow and Adipose Tissue-Derived Stem Cells. *Advanced Healthcare Materials* **2014**, *3*, 115-125.

(57) Livak, K. J.; Schmittgen, T. D. Analysis of Relative Gene Expression Data Using Real-Time Quantitative PCR and the 2−ΔΔCT Method. *Methods* **2001**, *25*, 402-408.

TABLE OF CONTENTS/ABSTRACT GRAPHIC